

Study on the Properties of Micro - arc Oxidation Self - assembled Composite coatings on Magnesium Alloy

Wei Shang^{1,2}, Yuanyuan Wang¹, Yuqing Wen^{1,*}, Xiaoqiang Zhan¹, Dan Kong¹

¹ Guangxi Key Laboratory of Electrochemical and Magnetochemical Function Materials, Guilin University of Technology, Guilin, 541004, China

² Collaborative Innovation Center for Exploration of Hidden Nonferrous Metal Deposits and Development of New Materials in Guangxi, Guilin University of Technology, Guilin, 541004, China

*E-mail: wenyuqing16@163.com

Received: 27 July 2017 / Accepted: 22 September 2017 / Published: 12 November 2017

The micro-arc oxidation / bis[(γ -triethoxysilyl)propyl]tetrasulfide (BTESPT) self-assembled composite coatings were prepared on the surface of magnesium alloy by self-assembly (SAM) and micro-arc oxidation (MAO). The surface morphology and composition of the composite coatings were characterized by scanning electron microscopy (SEM) and energy dispersion spectrometry (EDS). The corrosion resistance of the composite coatings was studied by electrochemical impedance spectroscopy (EIS), polarization curves and the experiments of immersion. The test results showed the anti-corrosion of the composite coatings were significantly improved compared with the pure micro-arc oxidation film. The formation mechanism of the self-assembled membrane on the micro-arc oxidation layer of magnesium alloy was investigated by dynamic simulation. The results showed that the self-assembled molecules were chemically adsorbed on the solid surface.

Keywords: Magnesium alloy, Micro-arc oxidation, Self-assembly, corrosion resistance, Dynamic simulation

1. INTRODUCTION

Magnesium and its alloys have many excellent physical and mechanical properties, such as the lowest densities among metals and high specific strength, etc. This is the reason why the magnesium alloy can be widely researched and applied in automotive, aerospace, computer industry and so on [1-3]. However, the magnesium-based materials have poor corrosion resistance which is the major obstacle of the use of it. Therefore, the corrosion protection of magnesium alloys is essential.

There are many methods to be applied to the magnesium alloys, such as chemical conversion films, micro-arc oxidation, self-assembly, organic coatings, etc. At present, the micro-arc oxidation (MAO) and self-assembly technique are the research hotspot for the surface treatment technology of magnesium alloys. Micro-arc oxidation technology is developing based on the traditional anodic oxidization and is a promising surface treatment method to produce protective film which firmly adheres on the substrates [4-7]. Unfortunately, a lot of micro-pores and micro-cracks were appeared on the surface of Mg alloy MAO film due to the use of a continual and intense sparking discharge and gas bubbling. The results showed that MAO had some defects for the corrosion protection of magnesium alloys.

With the maturity of self-assembly technology, it is widely applied in many areas, especially in the metal surface treatment [8-10]. Compared with the traditional membranes, self-assembled membrane will not appear the phenomena of brittle, aging, discoloration and is very suitable for metal protection [11]. In addition, it has the properties of small toxicity, simple operation, chemical stability and so on. As the follow-up process of micro-arc oxidation film, self-assembly which have a certain hydrophobic action can be seal the micro-pores and micro-cracks on the surface of micro-arc oxidation layer. It was effective to separate the Mg substrate from the corrosive medium [12-14]. Consequently, the corrosion resistance of the composition coatings was much better than the pure micro-arc oxide layer.

2. EXPERIMENTAL SECTION

2.1. Materials and preparation of membrane

In the experiment, the AZ91 magnesium alloy was employed with the following composition (wt.%): Al 9.4, Mn 0.23, Zn 0.82, Fe 0.005, Si 0.01, Ni 0.002, Cu 0.02 and Mg balance. The magnesium alloy was machined into a size of 30 mm × 20 mm × 2 mm and then the substrate was polished with 280 #, 600 #, 800 # and 1200 # water abrasive paper and rinsed with plenty of distilled water. The magnesium alloy was put into alkaline degreasing (40 g·L⁻¹ Na₂CO₃, 20 g·L⁻¹ Na₃PO₄, 20 g·L⁻¹ NaOH) for 60s, and then rinsed with distilled water again. Subsequently, the magnesium alloy was successively cleaned in an ultrasonic bath of absolute ethanol solution and distilled water for 10min. The treated magnesium alloy was dry in an oven of 50 °C.

The JHMAO-380/20A micro-arc oxidation power supply was employed to the process of MAO. In this work, magnesium alloy as the anode and stainless steel sheet as the cathode were put in the electrolyte of the silicate solution (4~6 g·L⁻¹ Na₂SiO₃, 8~10 g·L⁻¹ NaF, 10~12 g·L⁻¹ NaOH) at voltage increasing to 180~220 V. Pulse frequency and the duty cycle were fixed at 50 Hz and 30%. Afterward the sample was washed with distilled water and placed in a blast oven for drying with a temperature of 40 °C.

Here, the micro-arc oxidation self-assembled composite coatings were prepared. The methanol, BTESPT solution and distilled water were mixed thoroughly at a volume of 10: 1: 1 to prepare a self-assembled solution. Bis[(γ-triethoxysilyl)propyl]tetrasulfide is a low molecular organosilicon

compound which is commonly known as silane coupling agent Si-69. [15] It is commonly used in the treatment of carbon black, SiO_2 and other inorganic fillers. It not only has the role of activator, coupling agent, but also has the role of cross-linking agent, softener and reinforcing agent. And it is used as a reinforcing agent and a vulcanizing agent in the rubber industry [16]. The pH of the self-assembled solution was 3.5 (Acetic acid was used to adjust the pH). The self-assembled solution was stirred at 50 °C for 4 hours and then quietly placed for 2 hours. Next, the micro-arc oxidized magnesium alloy sheet was slowly placed in a self-assembly solution, immersed at 50 °C for 40 minutes and the excess self-assembly solution was cleaned with distilled water. The sample was then dried in an oven at a temperature of 80 °C for one hour. With this processing, the composite coatings were prepared on Mg alloy surface.

2.2. Performance testing

2.2.1. Surface characterization

The surface morphology of the self-assembled and the micro-arc oxidation composite coatings of magnesium alloy was observed by JSM-6380LV scanning electron microscope. The cross-sectional structure and elemental composition of the different films were characterized by the S-4800 field emission scanning electron microscopy and the energy dispersion spectrometry (EDS) which was attached to the SEM. The XG-CAMA contact angle tester was used to measure the contact angle of each sample to illustrate the hydrophobic properties of each film.

2.2.2. Electrochemical performance test

The electrochemical impedance spectroscopy (EIS) and Tafel polarization curves of each sample were tested at room temperature using CHI860D electrochemical workstation. A three-electrode test system was used. The three-electrode arrangement used a saturated calomel electrode (SCE) as the reference electrode, a platinum electrode as the counter electrode and the sample as the working electrode. The electrochemical test of each sample was carried out in 3.5 wt.% NaCl solution and the exposed effective area was 1 cm². When the open circuit potential (OCP) is stabilized, the AC impedance test and the polarization curve test were performed in NaCl solution.

The AC impedance test parameters were as follows: a frequency range of 0.1 Hz to 100 kHz and a sinusoidal applied perturbation voltage of 10 mV were employed. After the test, Zview software was used to simulation the obtained AC impedance data.

Polarization curves were scanned on both sides of the open circuit potential. The scanning range was from $E_{\text{OCP}} - 200$ mV to $E_{\text{OCP}} + 200$ mV and the scanning rate was 0.5 mV·s⁻¹. The linear polarization resistance and corrosion current density of the samples were obtained by fitting the curves.

2.2.3. Immersion experiment

In order to further study the long-term anticorrosion performance of composite coatings, immersion test was used for it. The immersion solution was a 3.5 wt.% NaCl solution with a soaking

time of 120 h and the sample was taken out at intervals of 24 h. The surface corrosion process of the film was characterized by polarization curve test. The polarization curves were tested according to the method which above the electrochemical performance test.

2.2.4. Dynamic simulation of self-assembly behavior

In recent years, with the rapid development of computer technology, computer technology-based molecular dynamics simulation is widely used in the simulation study about the properties of material density, interfacial tension, material structure and so on. Molecular simulation technology plays an important role in a growing number of fields. This molecular simulation technology was employed to the study of self-assembly. It can be used to explain the mechanism of self-assembly and possible adsorption methods and determine the performance of the film. In this paper, the molecular dynamics (MD) simulation was performed using Discover module of Materials Studio 6.0 program developed by Accelrys Inc. The whole system was performed at 298 K controlled by the Andersen thermostat, NVT ensemble, with a time step of 1.0 fs and simulation time of 500 ps, using the DISCOVER force field [17, 18]. The size of the adsorption was determined by the magnitude of the adsorption energy and the radial distribution function was calculated to determine the type of adsorption, so that the self-assembly process could be further explained theoretically.

3. RESULT AND DISCUSSION

3.1. Surface performance

3.1.1. Surface morphology

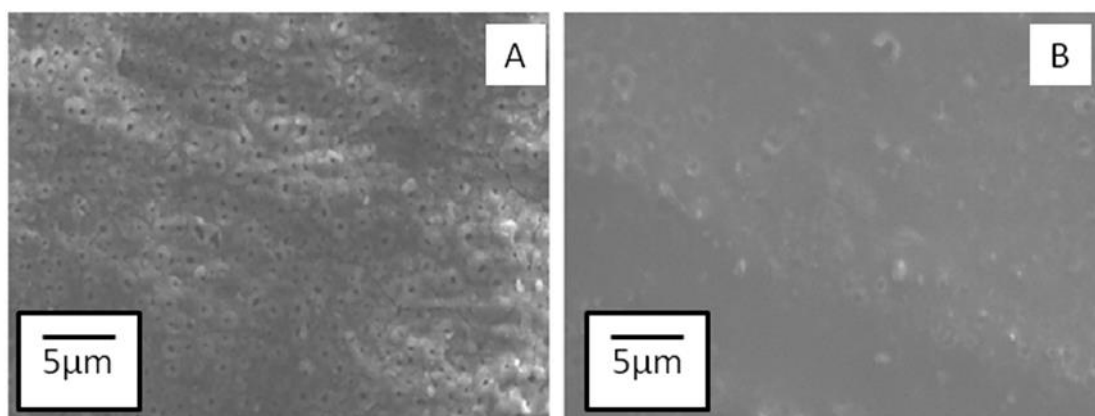


Figure 1. The surface morphology of micro-arc oxidation film (A) and composite coatings (B) on magnesium alloy.

SEM images of MAO film and composite coatings were shown in Fig.1. In Fig.1 (a), the micro-arc oxidation film of magnesium alloy had the porous structure. This structure which was the conventional morphology of MAO process called micro-arc channels were developed during the

micro-discharging time. These micro-pores were detrimental to corrosion resistance of the MAO film [19, 20]. In Fig .1 (b), the magnesium alloy composite coatings had the dense structure, but the microstructures produced by the micro-arc oxidation were also vaguely visible because of the thinner self-assembly layer. The self-assembled layer on the micro-arc oxide layer sealed the micro-pores produced by the micro-arc oxidation and forms a relatively uniform self-assembled layer.

3.1.2 Cross-sectional and energy spectrum analysis

In Fig.2 and Fig.3, the cross-section and energy spectrum of the micro-arc oxidation film and the composite coatings of magnesium alloy were shown, respectively. As shown in Fig.2, the composition of micro-arc oxidation film mainly was O, F, Mg and Si elements. Because Mg substrate was used to experiment, the Mg element is essential. The O element was generated due to micro-arc oxidation. A small amount of Na and Si element rooted from NaF and Na₂SiO₃ of the micro-arc oxidation electrolyte. As shown in Fig.3, the composition of the composite coatings also had the C and S elements in addition to the main components in the micro-arc oxidation film. C and S were the key elements of the BTESPT (C₁₈H₄₂O₆Si₂S₄) constituting the self-assembled membrane. Therefore, it could be explained that a self-assembled membrane had been formed on the micro-arc oxide layer of the magnesium alloy.

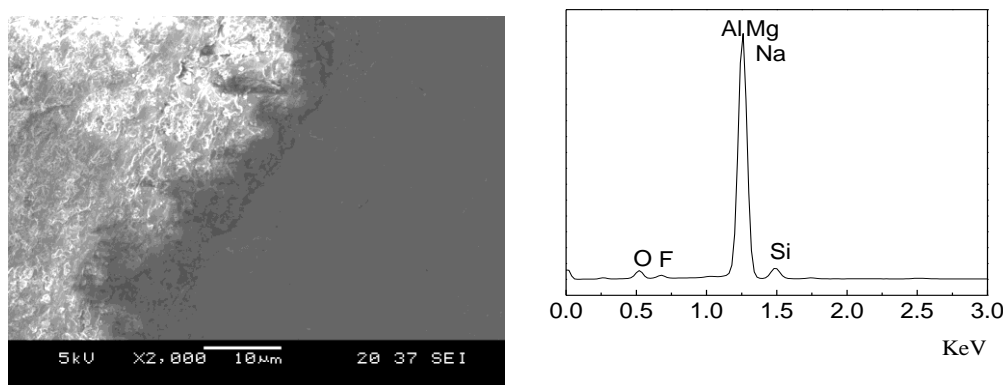


Figure 2. The cross-sectional morphology and composition of the micro-arc oxide film

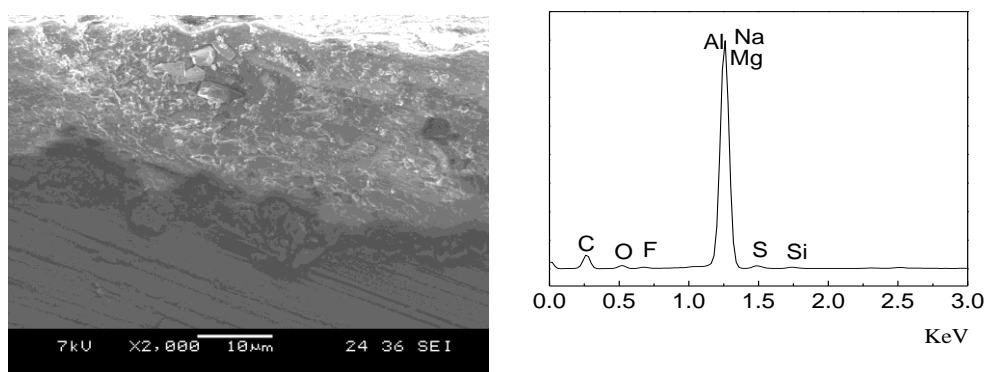


Figure 3. The cross-sectional morphology and composition of the micro-arc oxidation self-assembly composite coatings

3.1.3 Contact angle test

Fig.4 (A) showed the contact angle of the micro-arc oxidation film on the magnesium alloy. In the picture, the water droplet was approximately tiled and the contact angle was 44.09° . Fig.4 (B) showed the contact angle of composite coatings of magnesium alloy. It could be seen that the water droplet appeared semicircular on the surface and the contact angle was 80.67° . Because of the micro-porous structure, the surface of micro-arc oxidation film was rough and the surface of composite coatings was smooth after self-assembly process [21]. It could be seen that the hydrophobicity of the composite coatings had been improved remarkably, which mean the bilayer had a certain effect on improving the corrosion resistance of the composite coatings.

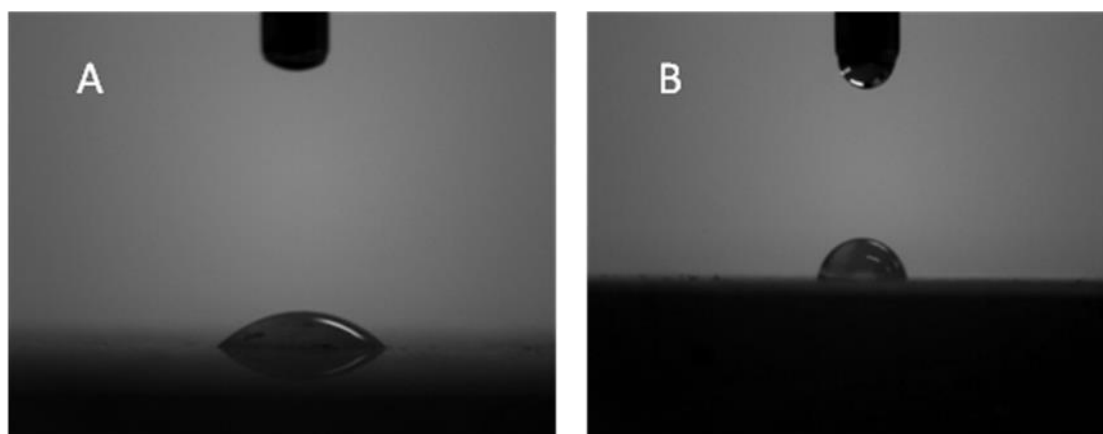


Figure 4. Contact angle measurements of micro-arc oxidation film (A) and composite coatings (B).

3.2 Electrochemical corrosion behavior

3.2.1 Characterizing by EIS

EIS measurements were often used extensively to evaluate the corrosion resistance of the film system. This technique not only compared the performance between different films, but also explained important information about the kinetics of film degradation and the corrosion process in corrosive media.

Fig.5 was AC impedance bode chart of the sample measured in a 3.5 wt.% NaCl solution. Fig.5 (A) was bode mold chart and Fig. 5(B) was bode phase angle chart. In bode mold chart, the high frequency region represented the resistance of the film to the penetration of the corrosion solution. The larger the resistance value, the better the density of the film. The middle frequency region represented the capacitance of the film. The linear relationship in the frequency range showed good capacitance which represents the film was relatively complete without serious corrosion damage. The low frequency region represented the corrosion resistance of the whole film. The larger the resistance value, the better the corrosion resistance of the film [22]. As could be seen in Fig.5, the micro-arc oxidation self-assembled composite coatings impedance values close to 10^6 orders of magnitude, which was larger than that of the micro-arc oxidation film, and the impedance value of the micro-arc

oxidation film was much larger than that of the blank magnesium alloy. The result demonstrated that compared with the micro-arc oxide film and the magnesium alloy substrate, the composite coatings had the lowest roughness and the best corrosion resistance.

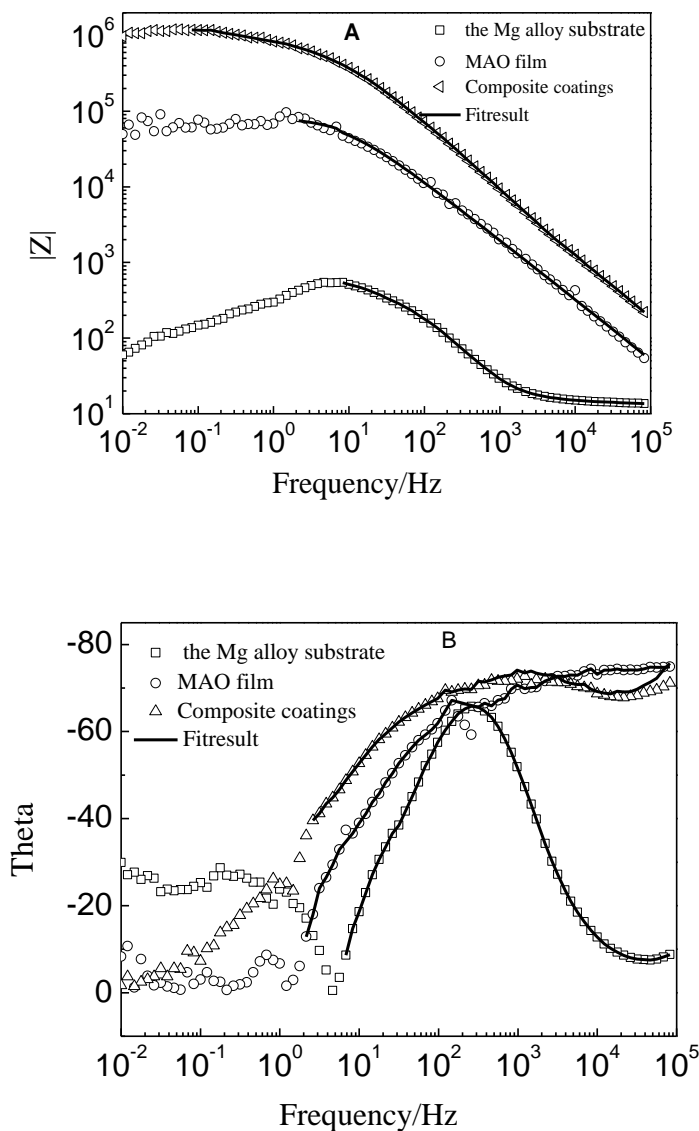


Figure 5. the Bode chart of AC impedance: bode mold chart (A) and bode phase angle chart (B) in a 3.5wt. % NaCl solution at room temperature

In order to quantitatively estimate the corrosion protection of the composite coatings, equivalent circuits were employed to simulate the experimental Bode diagrams, as shown in Fig.6. The bare magnesium alloy and the micro-arc oxide film could be represented by the equivalent circuit shown in Fig.6 (a), where R_s was the solution resistance between the working electrode and the reference electrode, also known as the liquid resistance, Q_{coat} was the capacitance of the micro-arc oxide film, and R_{coat} was the resistance of the micro-arc oxide film [23, 24]. The equivalent circuit of micro-arc oxidation self-assembled composite coatings was shown in Fig.6 (b), where Q_{coat} was the capacitance of the composite coatings, R_{coat} was the resistance of the self-assembled composite

coatings, Q_{dl} represented the capacitance of the bilayer, and R_{ct} was the interface bilayer charge transfer resistance.

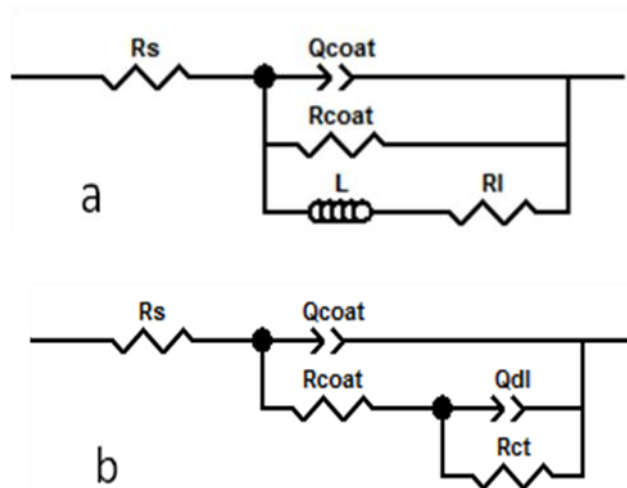


Figure 6. The equivalent circuits: MAO film (a) and composite coatings (b)

In the equivalent circuit, due to the effect of the non-uniform surface and diffusion, the capacitance C was replaced by the constant phase element (CPE) Q [25]. The general expression of the constant phase element impedance was [26-30]:

$$Z_{CPE} = 1/A(j\omega)^n$$

Where ω was the angular frequency ($\text{rad}\cdot\text{s}^{-1}$), j was the polarization current density ($\text{A}\cdot\text{cm}^{-2}$), A was the CPE constant ($\Omega^{-1}\cdot\text{s}^n\cdot\text{cm}^{-2}$). The n was a dimensionless index of CPE whose value was between 0 and 1. The roughness of the surface of the film affects the value of n . The smaller the n value was, the larger the Q_{coat} and Q_{dl} were. This indicated that the surface roughness of the electrode was more severe and the pitting was more likely to occur. On the contrary, it was not like that [31, 32].

According to the equivalent circuit, the AC impedance spectrum was fitted and the final fitting data could be well consistent with the measured EIS chart. The data were shown in Table 1.

Table 1. Fitting result for Bode plot

Sample	R_s ($\Omega\cdot\text{cm}^2$)	Q_{coat} (F/cm^2)	n_1	R_{coat} ($\Omega\cdot\text{cm}^2$)	Q_{dl} (F/cm^2)	n_2	R_{ct} ($\Omega\cdot\text{cm}^2$)
Mg alloy substrate	13.89	1.659×10^{-5}	0.895	536.1	–	–	–
MAO film	9.165	5.374×10^{-7}	0.783	84915	–	–	–
Composite coatings	2.662	5.118×10^{-8}	0.872	658920	5.996×10^{-7}	0.679	623590

It could be seen from Table 1, the impedance value of the bare magnesium alloy, the micro-arc oxidation film and the composite coatings was $5.361 \times 10^2 \Omega \cdot \text{cm}^2$, $8.4915 \times 10^4 \Omega \cdot \text{cm}^2$, and $6.589 \times 10^5 \Omega \cdot \text{cm}^2$, respectively. These results showed that the composite coatings could greatly improve the corrosion resistance of the magnesium alloy. The capacitance of the magnesium alloy, the micro-arc oxide film and the composite coatings was $1.659 \times 10^{-5} \text{F} \cdot \text{cm}^{-2}$, $5.37 \times 10^{-7} \text{F} \cdot \text{cm}^{-2}$, $5.51 \times 10^{-8} \text{F} \cdot \text{cm}^{-2}$, respectively. Their capacitance which became gradually smaller was agreement with the law of impedance values. As the micro-arc oxidation film was porous, although the film could be a good contact with the substrate, the surface was still rough. Compared with the micro-arc oxidation film, the n value of the composite coatings was increased to 0.872, indicating that the surface of the composite coatings was relatively smooth.

3.2.2 Polarization curve

Fig.7 showed the linear polarization curve of the magnesium alloy, the micro-arc oxidation film and the composite coatings. The data from the Tafel linear polarization curve were shown in Table 2. The corrosion potential represents the difficulty for the corrosion of the film, and the corrosion current density indicated the speed after the film started corrosion. From Table 2, it could be seen that corrosion potential of MAO film was smaller than that of the magnesium alloy, while the corrosion potential of the composite coatings were larger than that of MAO film. The reason was the surface of micro-arc oxide film has many micro-pores which were harmful to protecting the Mg alloy substrate. By comparison found that the corrosion current density of the composite coatings was smaller than the micro-arc oxidation sample and was much smaller than the bare magnesium alloy. Compared with the magnesium alloy, the corrosion current density of the composite coatings was reduced by three orders of magnitude. And compared with the micro-arc oxidation film, it was reduced by an order of magnitude. Therefore, the results of the polarization curve demonstrated that the composite coatings had better corrosion resistance than the micro-arc oxidation film and magnesium alloy substrate.

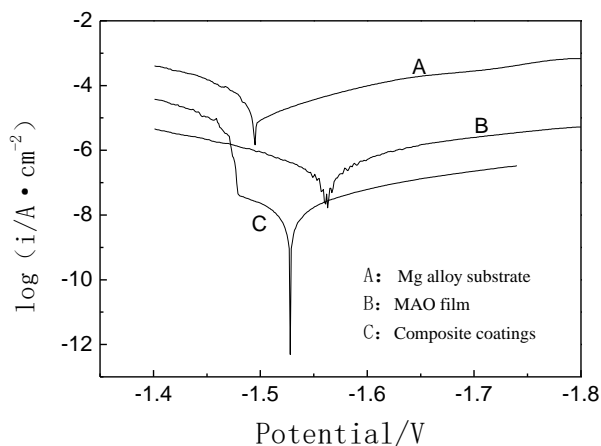


Figure 7. Potentiodynamic polarization curves of the Mg alloy substrate, MAO film and composite coatings in a 3.5 wt. % NaCl solution at room temperature

Table 2. The data from Tafel polarization curves of Figure 7.

Number	Corrosion potential/V	Corrosion current density /A·cm ⁻²
A	-1.4948	5.892×10 ⁻⁵
B	-1.5630	4.784×10 ⁻⁷
C	-1.5289	1.782×10 ⁻⁸

3.2.3 Study on immersion by dynamic potential polarization curve test

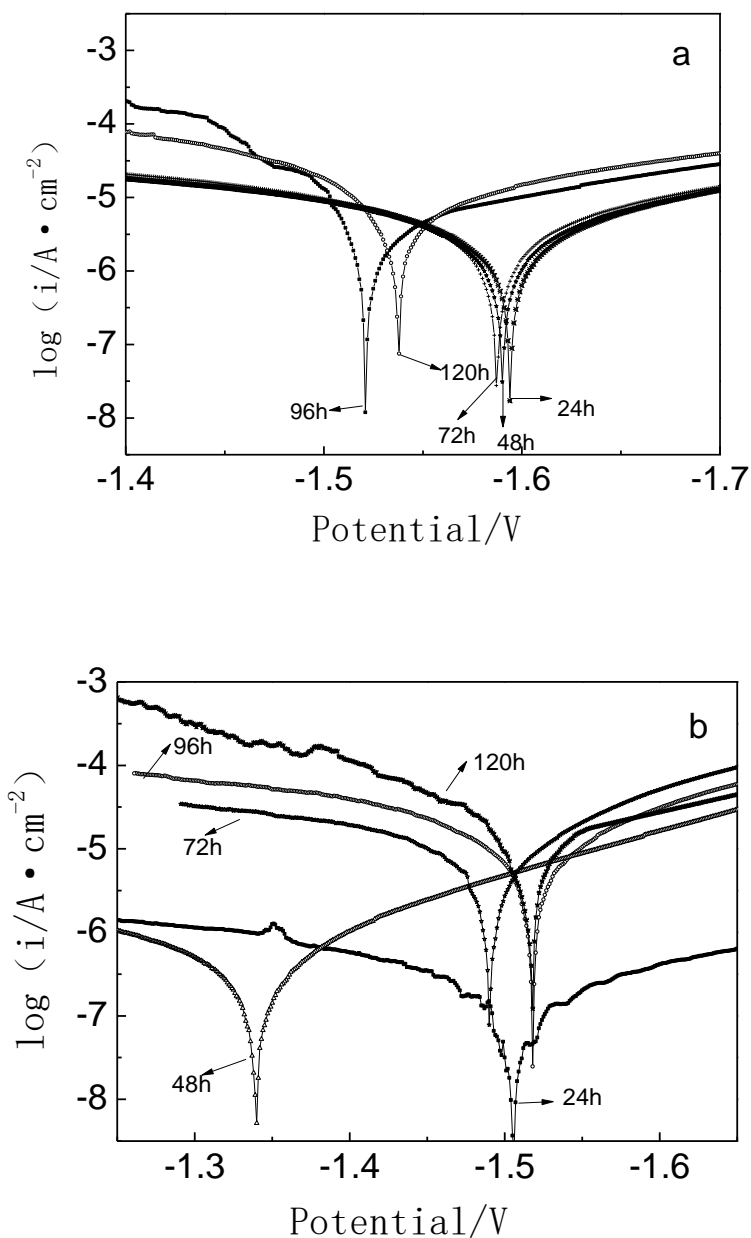


Figure 8. Potentiodynamic polarization curves of the MAO film (a) and composite coatings (b) at different immersion time in 3.5 wt.% NaCl solution at room temperature

Table 3. Parameter obtained from potentiodynamic polarization curves shown in Figure.8

Sample	Immersion time/h	Corrosion potential /V	Linear polarization resistance / Ω	Corrosion current density/ $A \cdot cm^{-2}$
MAO film	24	-1.594	9424.8	4.289×10^{-6}
	48	-1.590	9452.8	4.361×10^{-6}
	72	-1.587	9184.4	4.473×10^{-6}
	96	-1.521	4219.2	7.726×10^{-6}
	120	-1.538	3040.6	1.359×10^{-5}
Composite coatings	24	-1.506	186740.2	2.572×10^{-7}
	48	-1.340	71633.8	5.132×10^{-7}
	72	-1.490	3689.3	1.077×10^{-5}
	96	-1.518	2939.9	1.311×10^{-5}
	120	-1.518	1941.7	1.857×10^{-5}

Fig.8 showed the linear polarization curves of the micro-arc oxidation film and the self-assembled composite coatings immersed in 3.5 wt.% NaCl solution at different times. Table 3 showed a series of parameters obtained from Figure.8, such as corrosion potential (E_{corr}), corrosion current density (i_{corr}) and linear polarization resistance (R_p). The figure.8 and table 3 depicted that with the immersion time to extend, the corrosion current density of both the micro-arc oxidation film and the composite coatings were growing and the linear polarization resistance of them were getting smaller and smaller. The value of the corrosion current density was a key factor in evaluating the performance of the film. The smaller the corrosion current density was, the better the protective performance of the film. The greater the corrosion current density was, the worse the protective layer of the film. Simultaneously it was also an important indicator of the rate of corrosion reaction. The corrosion resistance of the micro-arc oxidation film was getting worse in the NaCl solution from the change of the current density of the micro-arc oxidation film and the self-assembled composite coatings. The possible reason was that the micro-arc oxidation film was damaged by the erosive Cl^- and water, leading to the rupture and dissolution of the film and then resulting in an increase in the area of corrosion. However, under the corrosion protection of the self-assembled composite coatings, the corrosion current density was lower by an order of magnitude than the MAO film. When the outer self-assembly layer was damaged after 72 hours, the corrosion current density became larger rapidly.

3.3 The result of dynamic simulation

The molecular structure of organic BTESPT was constructed by using Material Studio 6.0 software, and its structure was optimized. The optimized BTESPT molecule was shown in Fig.9.

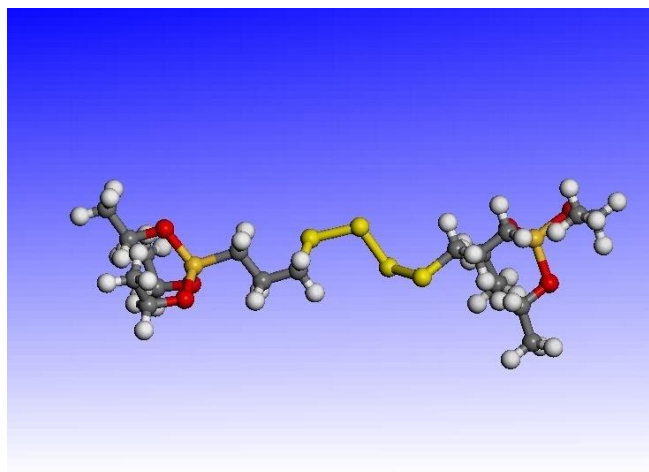


Figure 9. BTESPT molecules optimized

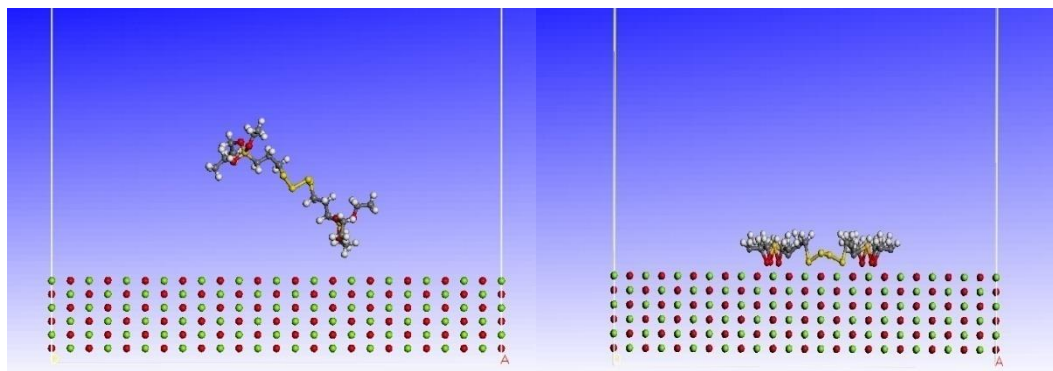
3.3.1 The adsorption model of BTESPT molecules was established on the crystal face of MgO (110), Mg(OH)₂ (110) and MgSiO₃ (110)

The interaction between the self-assembled molecules and the (110) crystal faces of the compounds was investigated by the mode of cutting facets. The constructed process resulted in minimizing the energy of the surface. [33-36] The effect of the thermal vibration of the surface atoms on the interfacial adsorption was negligible because its value was small, so all the atoms in the supercrystalline cell would be fixed. The optimal configurations of self-assembled molecules were simulated on MgO (110), Mg(OH)₂ (110) and MgSiO₃ (110), respectively. And the thickness of the vacuum layer of the supercrystal cell was 6.0 nm. The simulation details were shown in Table 4.

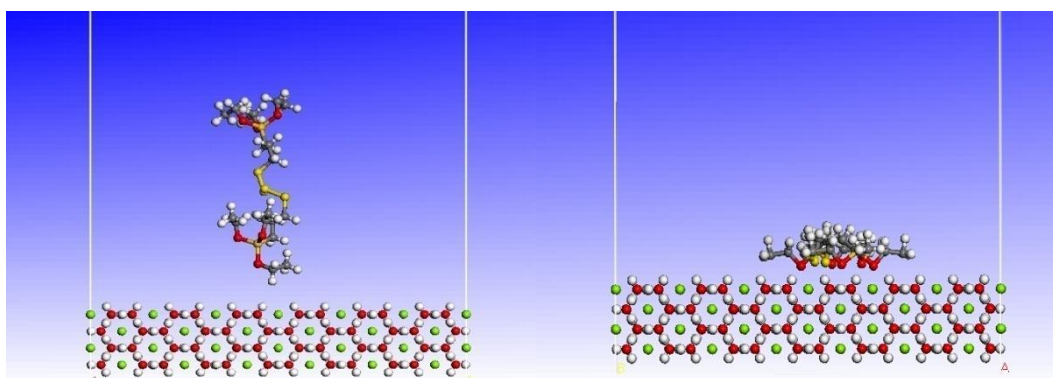
Table 4. The details of molecular mechanics and molecular dynamics simulations

Forcefield	non-bond	summation method	method	convergence level
compass	VdW, coulomb	Atom base, Ewald	smart minimizer	fine
maximum iterations	Ensemble	temperature	number of steps	time step
10000	NVT	298.0K	500000	1.0fs
Dynamics time	save	frame output every		
500.0ps	full	1000steps		

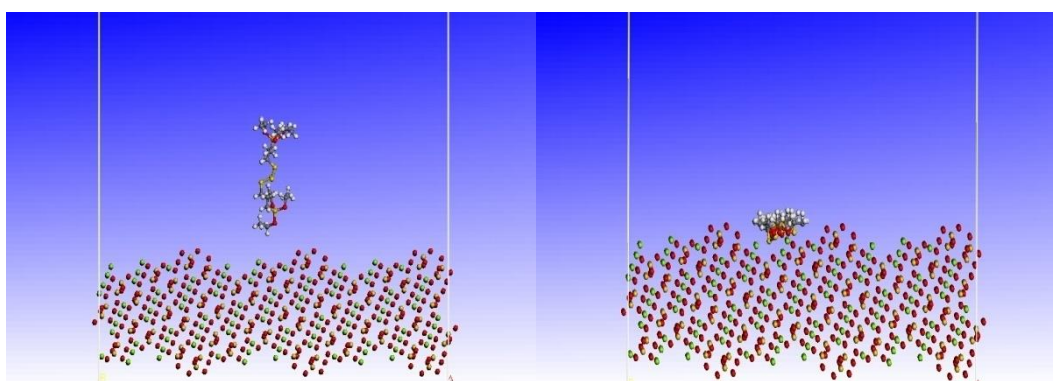
Fig.10 showed the final simulation results of the BTESPT organic molecules on MgO, Mg(OH)₂ and MgSiO₃. It could be seen that, no matter how to arrange the initial configuration, the BTESPT organic molecules could be well adsorbed on the various solid surface. This adsorption constructure not only made all of the -CH₃ distributed outside to improve the hydrophobicity of the self-assembled membrane, but also could effectively hinder the diffusion of the solution of H₂O, H⁺, Cl⁻ and other corrosive ions to the substrate surface to inhibit the corrosion of magnesium alloy.



(a) BTESPT in the MgO surface initial configuration (left) and adsorption configuration (right)



(b) BTESPT in the Mg(OH)₂ surface initial configuration (left) and adsorption configuration (right)



(c) BTESPT in the MgSiO₃ surface initial configuration (left) and adsorption configuration (right)

Figure 10. BTESPT with magnesium oxide, magnesium hydroxide and magnesium silicate surface molecules pharmacokinetic interactions is (a) (b) (c) respectively

The bond strength between self-assembled molecules and metal surfaces was an important measure of self-assembly performance. The adsorption of organic molecules on the metal surface could be calculated by the following formula:

$$E_{\text{adsorption}} = -E_{\text{interaction}} = -(E_{\text{total}} - E_{\text{surface}} - E_{\text{organ}})$$

Where $E_{\text{adsorption}}$ was the adsorption energy of organic molecules on the solid surface, E_{total} was the total energy of organic molecules and solid surface binding systems, E_{surface} and E_{organ} respectively represented the single point energy before the solid surface combined with the organic molecules. The adsorption energy was defined as the negative value of the interaction energy.

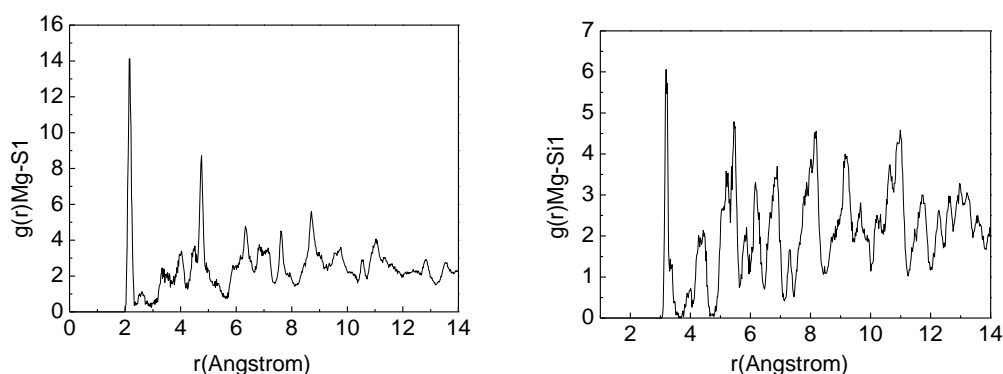
Table 5 listed the calculated data for the interaction of the self-assembled molecules with the solid surfaces. It could be seen that the adsorption energy of the self-assembled molecules on the surface of MgO, Mg(OH)₂ and MgSiO₃ was positive. The higher the value was, the easier the self-assembly solution combined with the surface and the better the corrosion resistance. Due to the (110) crystal face of MgO was relatively flat among these three substances, its surface adsorption energy was high to 42645.4 KJ • mol⁻¹.

Table 5. BTESPT with MgO, Mg(OH)₂, MgSiO₃ surface adsorption energy

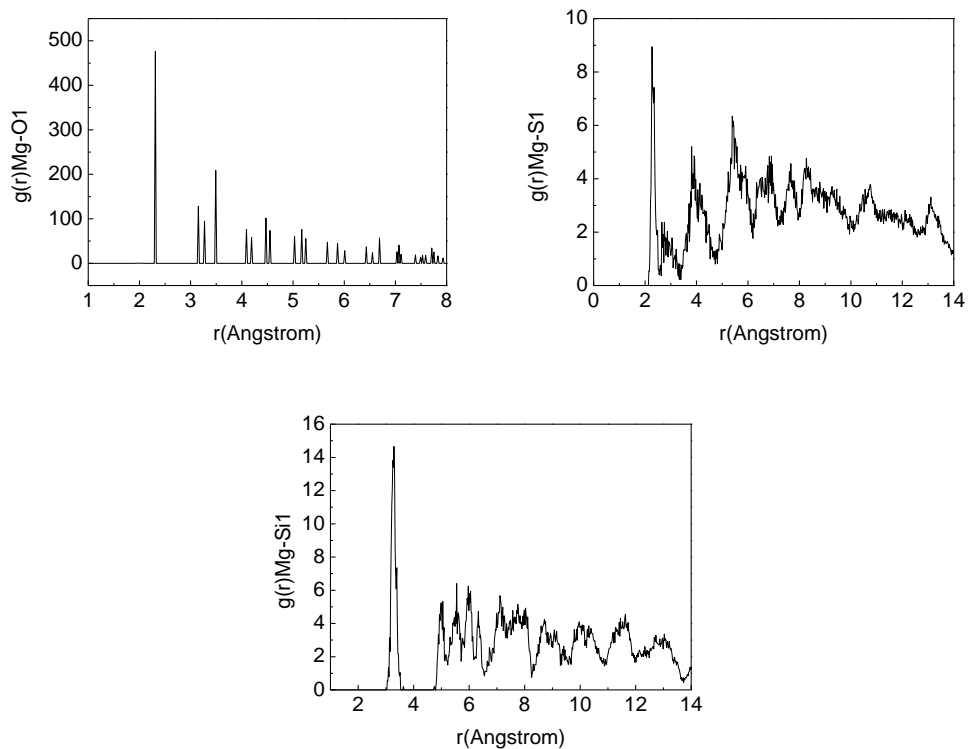
surface substrate	E _{total} KJ•mol ⁻¹	E _{organ} KJ•mol ⁻¹	E _{surface} KJ•mol ⁻¹	E _{interaction} KJ•mol ⁻¹	E _{adsorption} KJ•mol ⁻¹
MgO	47546629.9	11670.4	47577604.9	-42645.4	42645.4
Mg(OH) ₂	18609946.2	2473.2	18616965.7	-9492.7	9492.7
MgSiO ₃	31442659.2	6297.3	31459278.0	-22916.1	22916.1

3.3.2 Radial distribution function of molecular system

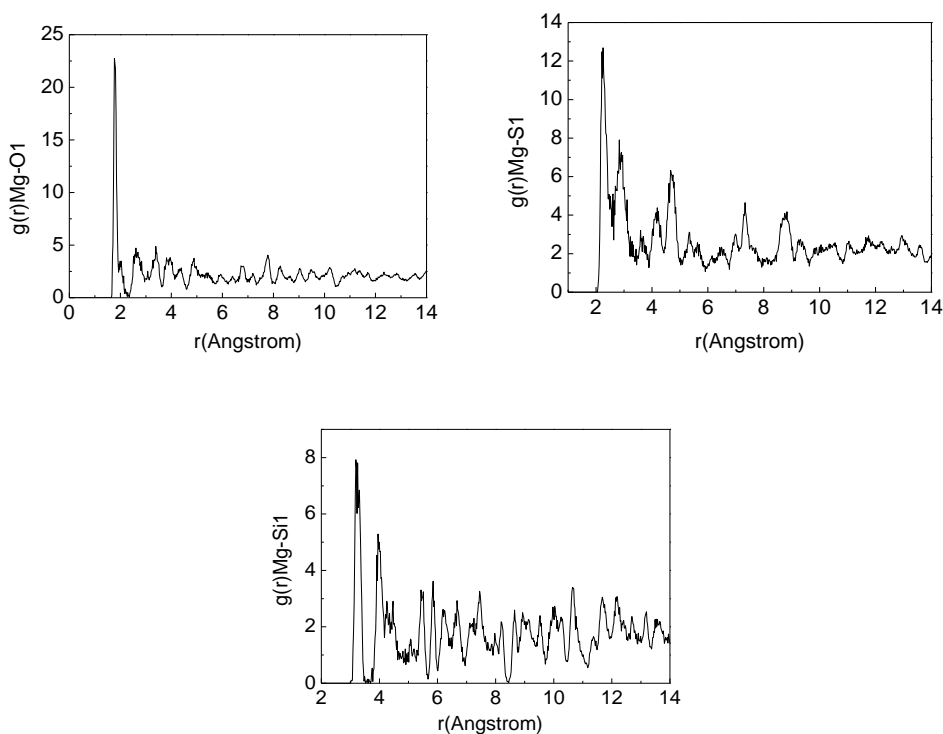
Radial distribution function was also called associative function. According to the final results of the molecular dynamics simulation of the organic molecules on the solid surface, the BTESPT molecules and the solid surface were taken as the analysis objects. The corresponding radial distribution function g (r) was obtained by analyzing the trajectories after the system equilibrium. In general, in the g (r) ~ r graphs the peaks before 3.5 Å were mainly composed of chemical bonds, hydrogen bonds, etc., and after 3.5Å it was mainly the interaction between the coulomb force and the vander Waals forces.



(a) The S, Si atom in BTESPT interaction between with MgO (110) face of a radial distribution function



(b) The O, S, Si atom in BTESPT interaction between with $Mg(OH)_2$ (110) face of a radial distribution function



(c) The O, S, Si atom in BTESPT interaction between with $MgSiO_3$ (110) face of a radial distribution function

Figure 11. BTESPT interaction between with MgO , $Mg(OH)_2$, $MgSiO_3$ of a radial distribution function

As could be clearly seen from Fig.11, the highest peak of each curve appears almost at a position of 3.5 Å. It revealed that the chemical bonds were formed between the O, S, Si which in the BTESPT with the surface, therefore the interaction of the surfaces was mainly chemical adsorption. It was agreement with the results of the adsorption energy calculations. It was also shown that the active groups which played a major role in the self-assembly solution were -S- and = Si =.

4. CONCLUSIONS

(1) The composite coatings were uniform and dense, and had the effect to seal micro-porous of the micro-arc oxidation film. The micro-arc oxidation film mainly contained elements such as O, F and Si, and the composite coatings mainly contained C, O, Si and S elements, which proved that the self-assembled membrane was existed on the surface of the micro-arc oxidation film. The results of the contact angle test illustrated that because of the hydrophobicity of the BTESPT molecules, the contact angle of the self-assembled composite coatings had a great improvement compared with the micro-arc oxidation film.

(2) The impedance value of the composite coatings was much larger than the magnesium alloy substrate and the micro-arc oxidation film, which indicated that the micro-arc oxidation self-assembled composite coatings had good corrosion resistance and achieves the purpose of improving the corrosion resistance of magnesium alloy. In addition, when the composite coatings were immersed in 3.5 wt.% NaCl solution for 120 hours, the surface of the sample was only slightly corroded, which also showed a better corrosion resistance of the micro-arc oxidation self-assembled composite coatings of magnesium alloy.

(3) BTESPT molecules were mainly attached to the micro-arc oxidation layer of magnesium alloy by chemical adsorption, which can effectively hinder the diffusion of ions such as chloride ions to the surface of magnesium alloy substrate and inhibit the corrosion of magnesium alloy.

ACKNOWLEDGEMENTS

This work was financially supported by National Natural Science Foundation of China (No. 51664011 and No.51665010), and the Project of Guangxi Key Laboratory Foundation of China (No. EMFM20171102).

References

1. P. Liu, X. Pan, W. Yang, K. Cai, Y. Chen, *Mater. Lett.*, 75(2012) 118.
2. X. Zhang, J. Yi, G. Zhao, L. Huang, G. Yan, Y. Chen, *Surf. Coat. Technol.*, 286(2016) 103.
3. X.-J. Cui, M.-T. Li, R.-S. Yang, Z.-X. Yu, *Appl. Surf. Sci.*, 363(2016) 91.
4. M. Sabaghi Joni, A. Fattah-alhosseini, *J. Alloys Compd.*, 661(2016) 237.
5. T. Qiu, X.L. Wu, F.Y. Jin, A.P. Huang, P.K. Chu, *Appl. Surf. Sci.*, 253(2007) 3987.
6. X.-J. Cui, R.-S. Yang, C.-H. Liu, Z.-X. Yu, X.-Z. Lin, *T. NONFERR. METAL. SOC.*, 26(2016) 814.
7. J. Han, P. Wan, Y. Sun, Z. Liu, X. Fan, L. Tan, *J. MATER. SCI. TECHNOL.*, 32(2016) 233.

8. Z. Grubac, M. Metikos-Hukovic, R. Babic, I.S. Roncevic, M. Petravic, R. Peter, *Mater. Sci. Eng. C Mater. Biol. Appl.*, 33(2013) 2152.
9. J. Huang, L. Zhou, *Carbohydr. Polym.*, 113(2014) 373.
10. G. Liu, S. Tang, D. Li, J. Hu, *Corros. Sci.*, 79(2014) 206.
11. X.G. Han, F. Zhu, X.P. Zhu, M.K. Lei, J.J. Xu, *Surf. Coat. Technol.*, 228(2013) S164.
12. S. Shen, Y. Zuo, *Corros. Sci.*, 87(2014) 167.
13. G. Qin, L. Fan, A. Watanabe, *J. Mater. Sci.*, 50(2014) 49.
14. X. Fan, J. Xu, Y. Wang, H. Ma, S. Zhao, X. Zhou, *Surf. Coat. Technol.*, 240(2014) 118.
15. L. Lei, J. Shi, X. Wang, D. Liu, H. Xu, *Appl. Surf. Sci.*, 376(2016) 161.
16. M.F. Montemor, M.G.S. Ferreira, *Electrochimi. Acta.*, 52(2007) 7486.
17. W. Shang, C. He, Y. Wen, Y. Wang, Z. Zhang, *RSC Adv.*, 6(2016) 113967.
18. W. Shang, X. Wang, Y. Wen, C. He, Y. Wang, L. Zhang, *PROT. MET. PHYS. Chem.*, 52(2016) 847.
19. M.A. Chen, Y.C. Ou, C.Y. Yu, C. Xiao, S.Y. Liu, *Surf. Eng.*, 32(2015) 38.
20. A. Golshirazi, M. Kharaziha, M.A. Golozar, *Carbohydr. Polym.*, 167(2017) 185.
21. Y. Chen, G. Yan, X. Wang, H. Qian, J. Yi, L. Huang, *Surf. Coat. Technol.*, 269(2015) 191.
22. S.-Y. Wang, N.-C. Si, Y.-P. Xia, L. Liu, *T. NONFERR. METAL. SOC.*, 25(2015) 1926.
23. C. Wang, B. Jiang, M. Liu, Y. Ge, *J. Alloys Compd.*, 621(2015) 53.
24. W. Shang, B. Chen, X. Shi, Y. Chen, X. Xiao, *J. Alloys Compd.*, 474(2009) 541.
25. S. Khorsand, K. Raeissi, F. Ashrafizadeh, *Appl. Surf. Sci.*, 305(2014) 498.
26. X. Guo, M. An, *Corros. Sci.*, 52(2010) 4017.
27. Z. Li, Y. Yuan, *RSC Adv.*, 6(2016) 90587.
28. D. Veys-Renaux, E. Rocca, J. Martin, G. Henrion, *Electrochimi. Acta.*, 124(2014) 36.
29. A.O. Yüce, G. Kardaş, *Corros. Sci.*, 58(2012) 86.
30. Y. Wang, Z. Huang, Q. Yan, C. Liu, P. Liu, Y. Zhang, *Appl. Surf. Sci.*, 378(2016) 435.
31. G.-L. Song, Z. Shi, *Corros. Sci.*, 85(2014) 126.
32. L. Song, Z. Chen, *Corros. Sci.*, 86(2014) 318.
33. Z. Zhang, N. Tian, X. Li, L. Zhang, L. Wu, Y. Huang, *Appl. Surf. Sci.*, 357(2015) 845.
34. Z. Zhang, N. Tian, L. Zhang, L. Wu, *Corros. Sci.*, 98(2015) 438.
35. Z. Zhang, N. Tian, W. Zhang, X. Huang, L. Ruan, L. Wu, *Corros. Sci.*, 111(2016) 675.
36. Z. Zhang, N.C. Tian, X.D. Huang, W. Shang, L. Wu, *RSC Adv.*, 6(2016) 22250.